Tracing the Star Formation Activity in the Most Distant Galaxies in the Universe

Christa DeCoursey, Eric Murphy, Eric Jimenez-Andrade
1. *National Radio Astronomy Observatory*
2. *University of Florida Department of Astrophysics*
(Dated: September 1, 2020)

We used deep Very Large Array (VLA) 3 and 6 GHz radio imaging of the *Hubble* Frontier Field (HFF) galaxy clusters MACSJ0416-2403, MACSJ0717+3745, and MACSJ1149+2223 to study star formation in gravitationally-lensed, intrinsically faint, high-redshift galaxies beyond the clusters. A stacking analysis is performed using μJy-level sensitivity and sub-arcsecond resolution (< 0.6") radio maps to derive the median star formation rates (SFRs) of galaxies out to z ≈ 9. Assuming Gaussian background noise levels in the stacked images allows for the calculation of SFR upper limits in these galaxies as a function of redshift. Galaxies are grouped in redshift bins 6 – 9 and 9 – 12. The upper limits for SFRs determined from the 3 GHz images as a function of redshift bin are, respectively, 52.92 and 322.39 $M_\odot$/yr at the three-sigma level. For the 6 GHz images, the SFR upper limits are, respectively, 191.64 and 743.50 $M_\odot$/yr at the three-sigma level. Our median-stacked images show only background noise rather than galaxy detections, meaning that μJy-level radio surveys are insufficient to probe the radio emission of z > 6 galaxies even after applying stacking analysis. We require deeper radio observations with R.M.S. < 1 μJy/beam from future astronomical radio facilities such as ngVLA and SKA to study the radio emission of z > 6 galaxies.

1. INTRODUCTION

Radio observations are useful probes into stellar evolution in distant galaxies as they provide dust-unbiased views into galactic properties such as SFR (Bera et al. 2018). While UV observations are also used to determine SFRs (To et al. 2014), they are obscured by dust and thus are biased towards lower SFRs. Using radio observations to derive SFR avoids this extinction bias, and these unbiased SFRs can be compared to the dust-biased SFRs from UV observations to determine extinction factors (To et al. 2014).

Radio imaging is particularly useful for determining SFRs because HII regions around young massive stars emit free-free radiation in radio frequencies, and supernova explosions of massive stars emit synchrotron radiation in radio frequencies. The existence and explosion of massive stars indicates current star formation because massive stars live for such short periods of time and new stars form from supernova debris. Synchrotron emission is the dominant form of emission up to a rest-frame frequency of roughly 30 GHz, and the synchrotron frequencies are red-shifted to our desired frequencies of 3 and 6 GHz for z < 6. Beyond roughly 30 GHz, free-free emission is the dominant form of emission and its rest-frame frequency is red-shifted to 3 and 6 GHz for z > 6.

Because radio emission is so useful for studying SFRs, many deep radio surveys have been conducted with the VLA to study star formation in high-redshift galaxies such as the VLA-COSMOS survey (Schinnerer et al. 2010; Smolcic et al. 2016) and JVLA imaging of GOODS-N at 20 cm (Owen 2018). However, even with current deep radio surveys, little is known about the radio properties of z > 6 galaxies. We therefore combine the power of gravitational lensing with deep radio maps provided by the VLA HFF survey to explore the radio properties of extremely faint, z > 6 galaxies.

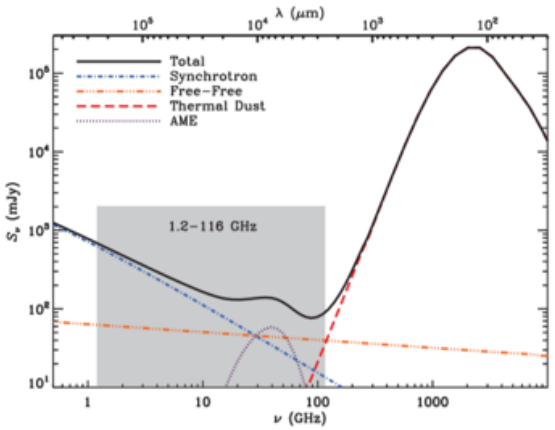

FIG. 1: The dominant form of radio emission as a function of rest-frame frequency. We rely on synchrotron radio emission for z < 6 galaxies and free-free radio emission for z > 6 galaxies (Murphey et. al. 2018).

The *Hubble* Frontier Field observational campaign used the *Hubble* Space Telescope (*HST*) and *Spitzer* Space Telescope to observe six massive galaxy clusters and their parallel fields in frequencies ranging from sub-mm to x-ray (Lotz et. al 2017). It used gravitational lensing from the dark matter in the clusters to magnify extremely faint or high redshift galaxies (2 < z < 12) that lie beyond the clusters. The high redshift galaxies are too intrinsically faint to yield any information about their properties, so the magnification associated with the gravitational lensing is necessary to study these galaxies. The VLA Frontier Fields survey targeted three of the HFF galaxy clusters - MACSJ0416, MACSJ0717, and MACSJ1149 - using 3 GHz and 6 GHz imaging with a resolution of ≈0.6 arcsec and a noise R.M.S. of ≈1 μJy/beam to produce deep radio maps (Heywood et al.

in prep).

The purpose of the project is to use the 3 and 6 GHz radio maps of the VLA Frontier Field survey to determine dust-unbiased median SFRs of massive high-redshift galaxies. Combining the effects of gravitational lensing to magnify distant galaxies and stacking to increase signal-to-noise ratio allowed us to derive SFR upper limits for some of the most distant galaxies in the universe.

This report of our project is organized as follows: In Section II, titled Data Analysis, we explain how we manipulated the radio cluster images to create our final stacked images and we explain how we converted the background noise of the stacks to upper limits for SFR. In Section III, titled Results, we list the upper limits for the median SFRs derived for each redshift bin and frequency combination, and we show graphs of these SFRs as a function of redshift. In section IV, titled Discussion and Future Steps, we discuss the limitations of our study and describe the future steps we need to take to determine actual SFRs for the high redshift galaxies rather than just upper limits.

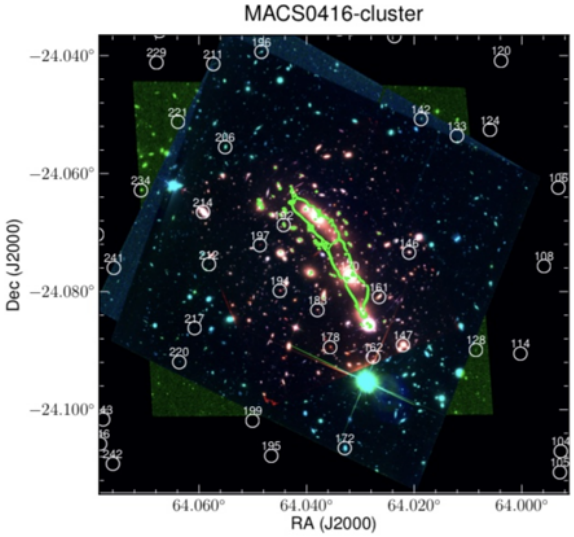

FIG. 2: HFF MACSJ0416 cluster (Jimenez-Andrade et al. in prep)

2. DATA ANALYSIS

The 3 GHz and 6 GHz VLA maps used in the stacking analysis have a resolution of ≈0.6 arcsec and a noise R.M.S. of ≈1 μJy/beam (Heywood et al. 2020). We convolved each of the original cluster images to a 1x1 arcsec beam with a position angle of 0 degrees so that the each image had the same synthesized beam shape. Convolving the images allowed us to stack cutout galaxies images from different clusters together. We used NRAO's CASA software to complete this convolution process. We also used CASA software to re-grid the original 6 GHz images to the 3 GHz image pixel scale of 0.16 arcsec/pixel. The original 6 GHz image pixel scale was 0.05 arcsec/pixel. Re-gridding the 6 GHz images to the pixel scale of the 3 GHz images allowed us to stack cutout galaxy images of differing frequencies together.

We used right ascension (RA) and declination coordinates from the VLA HFF survey to isolate thousands of 10x10 arcsec images centered upon the extremely faint, high-redshift galaxies from the cluster images (Shipley et al. 2018; Kawamata et al. 2018). We isolated these cutout images from the cluster images using the 2DCutout Python module. The Shipley catalog (Shipley et al. 2018) contains coordinates for galaxies with redshift 0 – 12 and the Kawamata catalog (Kawamata et al. 2018) contains coordinates for galaxies with redshift 6–9. We wrote a cross-matching script, validated via TopCat, to determine which sources existed in both the Shipley and Kawamata catalogs and ensure that these sources were only isolated from the cluster images once. Figure 2 shows the MACSJ0416 cluster.

We used median-stacking (Garn et al. 2018; Lindroos et al. 2018) to study the galaxies in the cutout images, as they are still too intrinsically faint to be studied individually even with the gravitational lensing magnification factors. Stacking allows us to study the median properties of these high-redshift galaxies as stacking increases the signal-to-noise ratio. Theoretically, the stacked image noise level decreases as a factor of $1/\sqrt{N}$ (Garn et al. 2018). We separated the cutout images into redshift bins of 6 – 9 and 9 – 12 prior to stacking them so we could eventually study galactic properties as a function of redshift.

We also considered using mean stacking but, along with other studies (Garn et al. 2018), we found that median stacking is more reliable because mean stacks can be biased towards bright sources or artifacts in the field. As a comparison between median and mean stacking, we created mean and median stacked images using the same 1000 sources detected above the 5-sigma level in the VLA HFF maps (Heywood et al. 2020). These stacks not only provided evidence for the reliability of median stacking, but also demonstrated that the stacking script worked in general. Figure 3 shows an example of one of these stacks. We evaluate the robustness of the stacking script by comparing the value of the central pixel of the stacked images and the resulting median/mean stack. We determined that median stacking is more reliable than mean stacking by comparing the expected R.M.S. noise levels, calculated via $1/\sqrt{N}$, to the noise level determined via a sigma clipping script. This script assumed Gaussian background noise and measured the background noise without considering pixel values that were greater than 3 standard deviations above the center Gaussian pixel value. This test yielded a closer comparison between the expected and measured noise levels for the median-stacked images than the mean-stacked images, thus showing that median stacking is more reliable.

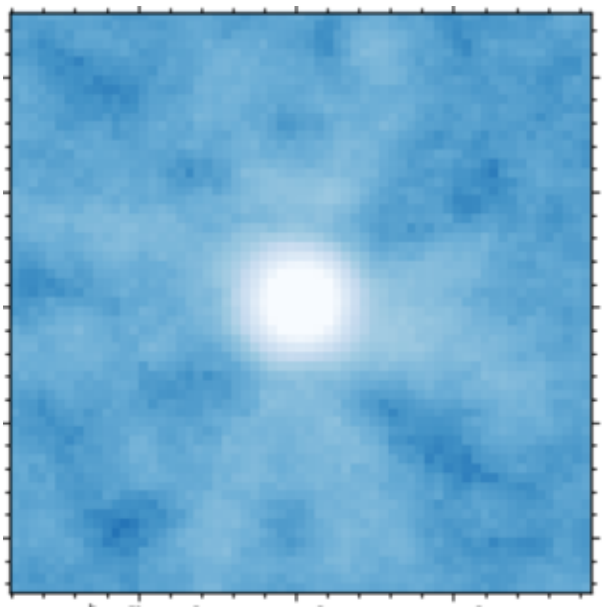

FIG. 3: This is a median-stacked image of 1000 strong 6 GHz galaxy detections from the MACSJ0416 HFF VLA cluster image.

For redshift bin 6 – 9, we included 391 and 302 cutout images in the 3 GHz and 6 GHz stacks, respectively, and for redshift bin 9 – 12, we included 43 and 37 cutout images in the 3 GHz and 6 GHz stacks, respectively. None of these four stacks showed any galaxy detections, and so to derive upper limits for their SFRs, we relied on the Gaussian background noise levels. We obtained the noise levels via the sigma clipping script with a cutoff level of 3. We are able to convert the R.M.S. background noise levels to upper limits for SFR in $M_\odot$/yr using the following equations (Murphy et al. 2011; Murphy et al. 2006a; Murphy et al. 2006b):

$$\left(\frac{\mathrm{SFR_{3\ GHz}}}{\mathrm{M_{solar}\ yr^{-1}}}\right) = 4.87\mathrm{x}10^{-29}\left(\frac{\mathrm{L_{1.4\ GHz}}}{\mathrm{erg\ s^{-1}\ Hz^{-1}}}\right). \quad (1)$$

$\mathrm{L_{1.4\ GHz}}$ is given by

$$\mathrm{L_{1.4\ GHz}} = \frac{4\pi \mathrm{D_L(z)}^2}{(1+\mathrm{z})^{1-\alpha}}\left(\frac{1.4}{3}\right)^{\alpha}\mathrm{S_{3\ GHz}}. \quad (2)$$

These equations apply to the 3 GHz frequency; to determine upper limits for SFR from the 6 GHz images, we changed the 3 to a 6 in equation 2 and we changed $\mathrm{S_{3GHz}}$ to $\mathrm{S_{6GHz}}$. α is 0.70 and we assumed a ΛCDM cosmology when calculating the luminosity distance as a function of redshift. We used the median redshift associated with the sources in each redshift bin as z, and we use the measured background noise levels obtained from the sigma clipping script for S.

z	Freq	N	Expected Noise	RMS Noise	Median Mass
6-9	3	391	5.06E-08	7.64E-08	8.23
6-9	6	302	5.18E-08	1.74E-07	8.29
9-12	3	43	1.53E-07	2.32E-07	8.86
9-12	6	37	1.48E-07	3.30E-07	8.25

TABLE I: This table compares the expected ($1/\sqrt{\mathrm{N}}$) R.M.S. noise versus measured R.M.S. noise (sigma clipping script) for the high-redshift bins. These noise values are in units of Janskys. It also lists the median mass of the galaxies involved in the stack in exponential units of solar masses.

3. RESULTS

Each of the high-redshift stacks, pictured in the Appendix, show only background noise. Figure 4 shows the Gaussian background noise contained in the redshift bin 6 – 9, 3 GHz image. A white blob in the center of the image would indicate a galaxy detection, but there is no blob and a histogram of the stack's pixel values was well-fit by a Gaussian, meaning that the stack is entirely noise.

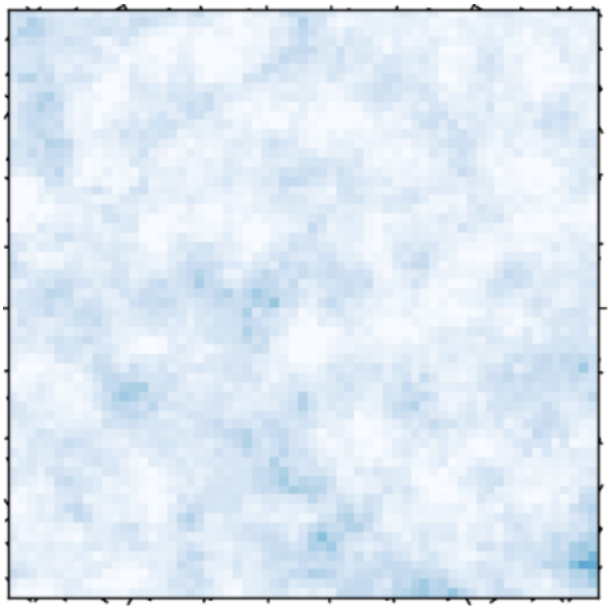

FIG. 4: This is the redshift bin 6−9, 3 GHz image. It has 391 sources stacked and contains no detection. It shows Gaussian-distributed background noise.

Table 1 lists the expected noise, calculated via $1/\sqrt{\mathrm{N}}$, the measured noise determined from the sigma clipping script, and the median mass in exponential solar mass units for the high-redshift bins. The measured R.M.S. noise values were used in equation (2) to determine upper limits for the luminosity of the galaxies.

z Bin	3 GHz SFR	6 GHz SFR
6-9	52.92	191.64
9-12	322.39	743.50

TABLE II: This table lists the upper limits for the median SFRs in $M_\odot$/yr for each redshift bin and frequency combination.

Table 2 lists the upper limits for the median SFR for the high-redshift bins as calculated the background R.M.S. noise using equations (1) and (2). The SFRs are listed in units of $M_\odot$/year.

Because we did not have any detections for the high redshift bins 6–9 and 9–12, we decided to stack sources in lower redshifts. As a first test, we stacked 1000 sources at redshifts 2 – 4 and 4 – 6 from the highest mass bins to ensure a robust detection. Only one of the four stacks, the 3 GHz stack for redshift bin 2 – 4, had a weak detection. Figures 5 shows this stack. The Appendix contains the remaining low-redshift bin stacks. We did not get strong detections at lower redshifts because we stacked very low mass star-forming galaxies which are expected to have low SFRs. However, if we stack higher mass galaxies and obtain detections, we will measure the flux via 2D Gaussian fitting and use this to determine actual SFRs rather than just upper limit estimates.

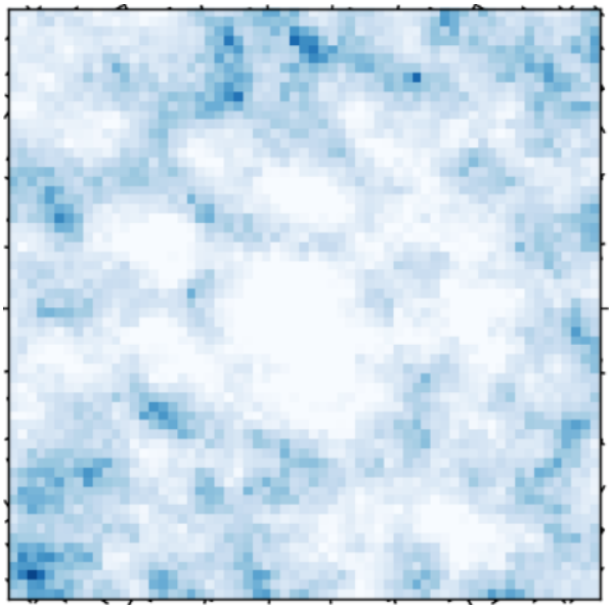

FIG. 5: This median-stacked image contains 1000 cutout galaxy images from the three galaxy clusters in the 3 GHz frequency. Each galaxy involved has a redshift between 2 and 4. The galaxies involved in the stack are the 1000 most massive galaxies in the redshift bin. The white blob in the center of the image is the detection.

The detection is weak but there is definitive evidence that the white blob in the center of the image is a detection. We assume that the background noise distribution is Gaussian, and so to determine if there is a detection, we plotted a histogram of the pixel values in the stack. If there is no detection and the image is entirely background noise, the histogram should be fit by a Gaussian. Figure 6 shows the pixel-value histogram of the 3 GHz image for redshift bin 2 – 4 on a logarithmic scale with a Gaussian fit applied. Clearly, there are higher pixel values that are not fit well by the Gaussian, indicating that there is a detection in the center of the image.

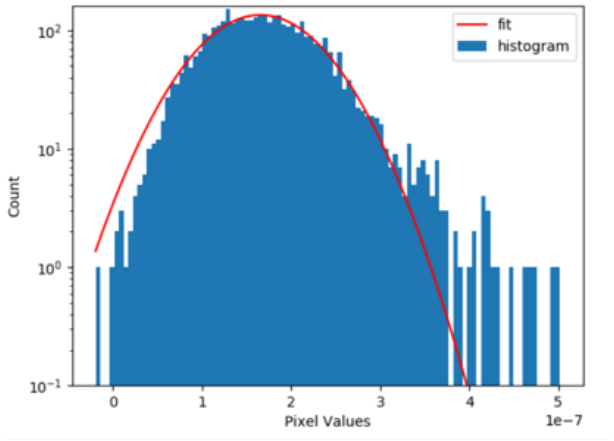

FIG. 6: This is the pixel-value (flux) histogram for the redshift bin 2 – 4, 3 GHz stacked image. If the image contained only background noise, the histogram would be fit well by a Gaussian. The existence of upper outliers in the histogram indicates a detection in the stacked image.

We determined SFR upper limits for the low redshift bins using equations (1) and (2) since we had no strong detections. Figure 7 shows SFR upper limits as a function of redshift for the 3 GHz images, and Figure 8 shows SFR upper limits as a function of redshift for the 6 GHz images. It remains unclear why the background noise from the 6 GHz images yield such higher upper limits for SFRs in the redshift bins.

The data points in Figures 7 and 8 lie at the intersection of the median redshift in each bin and the SFR as calculated from that median redshift. So, the data points lie towards the lower end of the redshift bins as lower redshifts are far more common than higher redshifts. The light and dark green data points provide SFRs for Lyman break galaxies at z = 4 based upon 1.4 GHz and UV dust-obscured data at the three-sigma level (To et. al. 2014). These data points fall below the upper limit for the SFR in redshift bin 4 – 6, so they support our upper limits for z = 4–6. SFRs based upon radio emissions have not previously been studied for redshifts greater than 6, so there are no prior results to compare our SFR upper limits to for these distant galaxies.

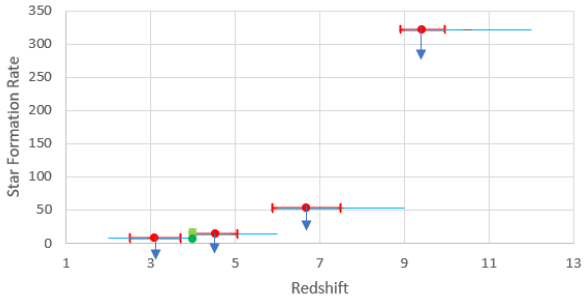

FIG. 7: Red: our data showing one standard deviation of redshift. Blue: the upper and lower limits of the redshift bins. Light Green: SFR for z≈4 galaxies using obscured 1.4 GHz data (To et. al. 2014). Dark Green: SFR for z≈4 galaxies using obscured UV data (To et. al 2014).

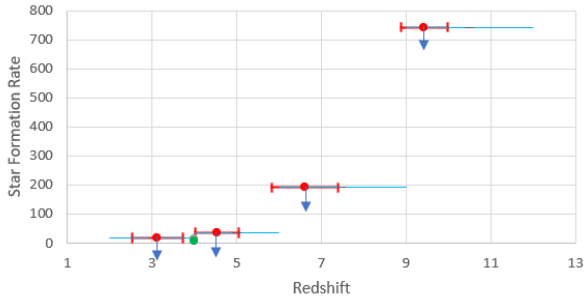

FIG. 8: Red: our data showing one standard deviation of redshift. Blue: the upper and lower limits of the redshift bins. Light Green: SFR for z≈4 galaxies using obscured 1.4 GHz data (To et. al. 2014). Dark Green: SFR for z≈4 galaxies using obscured UV data (To et. al 2014).

4. DISCUSSION AND FUTURE STEPS

While we would eventually like to estimate actual SFRs for $z > 6$ galaxies, it is promising that we have so far been able to establish upper limits for these SFRs. The SFR upper limits for redshift bin $6-9$ for the 3 GHz stack and 6 GHz stack are, respectively, 52.92 and 191.64 $M_\odot$/yr. The SFR upper limits for redshift bin $9-12$ for the 3 GHz stack and 6 GHz stack are, respectively, 322.39 and 743.50 $M_\odot$/yr.

If we are able to obtain detections as opposed to just background noise in our stacks, we will be able to derive SFRs rather than just upper limits. This is possible for redshift bins $2-4$ and $4-6$ once we determine how to stack more than 1000 images at a time. The weak detection for the 3 GHz redshift bin $2-4$ stack shows that we will be able to obtain detections for the lower redshift bins and use the flux density data to determine SFR as a function of redshift. Once we determine SFRs for each redshift bin, we will compare these SFRs to those determined from UV observations to determine extinction factors, as UV observations are dust-obscured while radio observations are not. Previous studies report 3.8 as the rest-frame UV extinction correction factor for Lyman break galaxies at $z \approx 4$ (To et. al. 2014).

The lack of detections in high-redshift bins implies that, even via stacking analysis, μJy-level radio surveys are still insufficient to probe the radio emission of $z > 6$ galaxies. One solution involves stacking more sources, but we currently do not have sufficient data to add more sources to the $z = 6-9$ and $9-12$ stacks. This forces us to explore alternative methods for studying $z > 6$ galaxies. We could carry out deeper observations, but that is observationally expensive with current facilities. Future radio astronomical facilities, such as the ngVLA and SKA, will be necessary to carry out these deeper observations. The VLA lacks frequency coverage for > 50 GHz where radio emission is dominated by free-free emission, but the ngVLA will cover these frequencies. This higher frequency free-free emission is essential for studying star formation in high-redshift galaxies and thus could potentially lead to detections in the higher redshift bins (Murphy et al. 2018). The Square Kilometer Array (SKA) will help us study signals below the survey threshold (Zwart et al. 2014).

Our radio study, while successful at deriving SFR upper limits for galaxies with $z > 6$, shows that more sophisticated radio astronomical facilities are necessary to study the radio continuum in distant galaxies.

References

Bera, A., et al 2018, IOP
Garn, T., et al. 2018, arXiv
Heywood, I., et al. in prep
Jimenez-Andrade, E., et al. in prep
Kawamata, R., et al. 2018, arXiv
Lindroos, L., et al. 2013, IAU
Murphy, E., et al. 2011, arXiv
Murphy, E., et al. 2018, ASP
Murphy, E., et al. 2006a, IOP
Murphy, E., et al. 2006b, IOP
Owen, F. 2018, IOP
Schinnerer, E. et al. 2010, IOP
Shipley, H., et al 2018, IOP
Smolcic, V., et al. 2016, EPD
To, C., et al 2014, IOP

Appendix

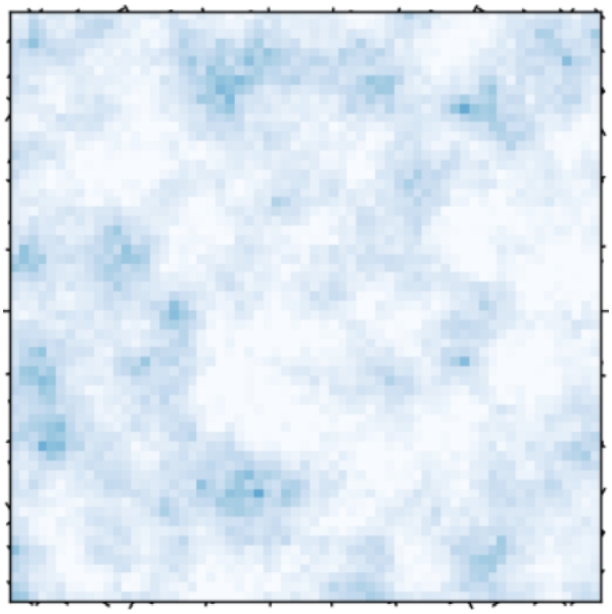

FIG. 9: 6 GHz, redshift bin 2 – 4, contains 1000 sources

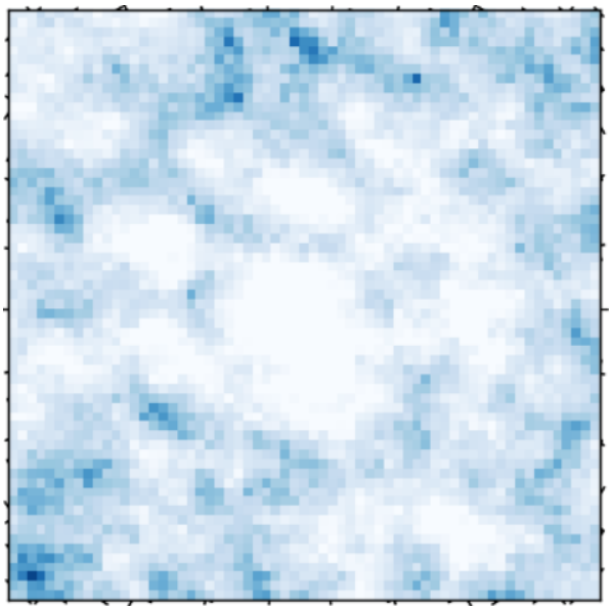

FIG. 10: 3 GHz, redshift bin 2–4, contains 1000 sources. This image contains a weak detection in the center.

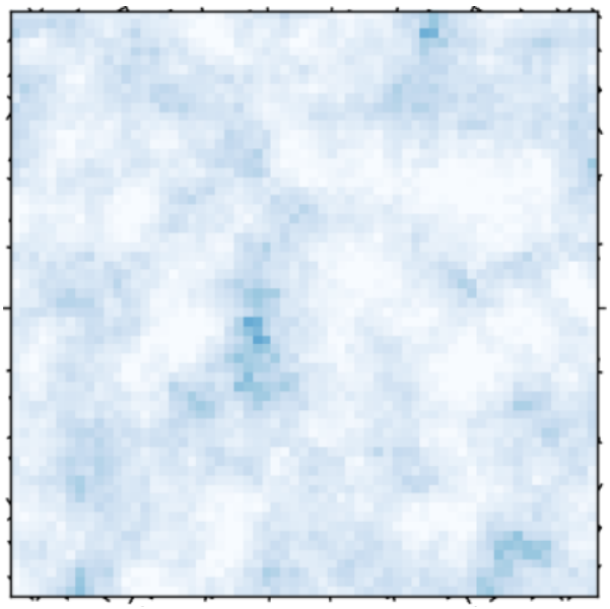

FIG. 11: 6 GHz, redshift bin $4-6$, contains 1000 sources

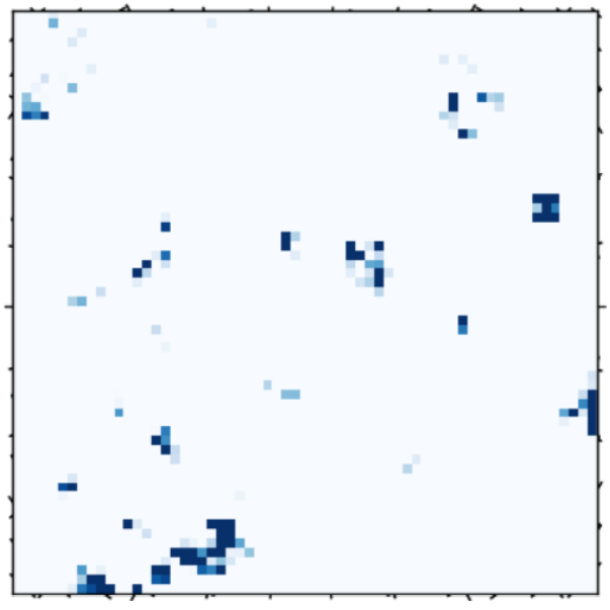

FIG. 12: 3 GHz, redshift bin $4-6$, contains 1000 sources. It is unclear why this image is more contrast than the others, but we suspect that one of the 1000 images involved in the stack contains a strong foreground source, so we need to eliminate that one image from the stack.

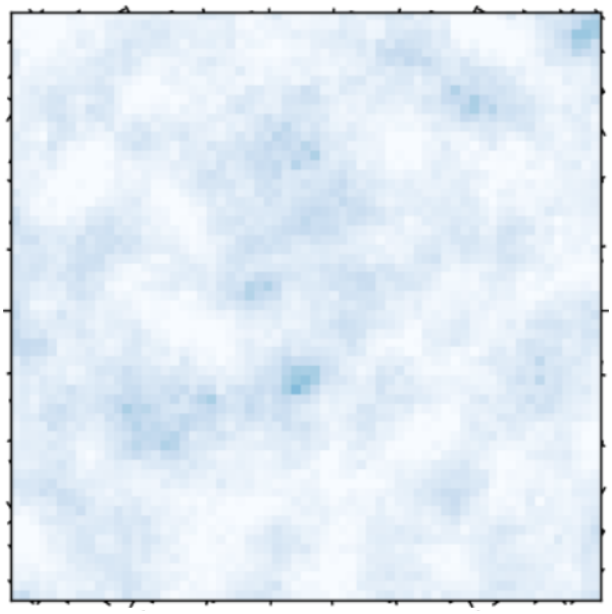

FIG. 13: 6 GHz, redshift bin 6 – 9, contains 302 sources

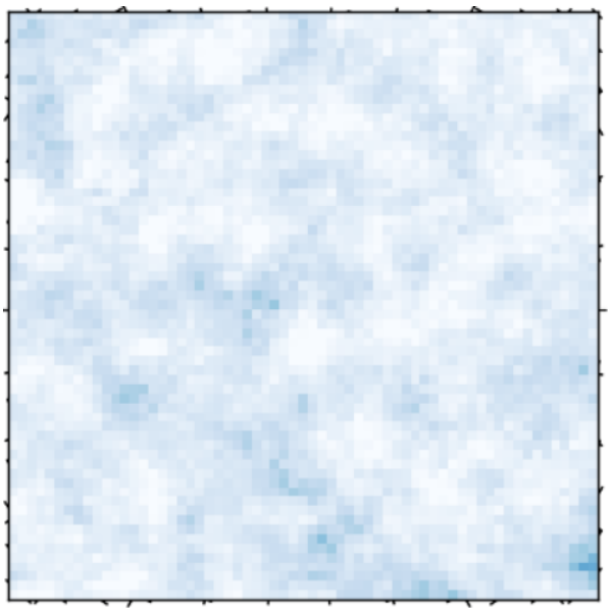

FIG. 14: 3 GHz, redshift bin 6 – 9, contains 391 sources

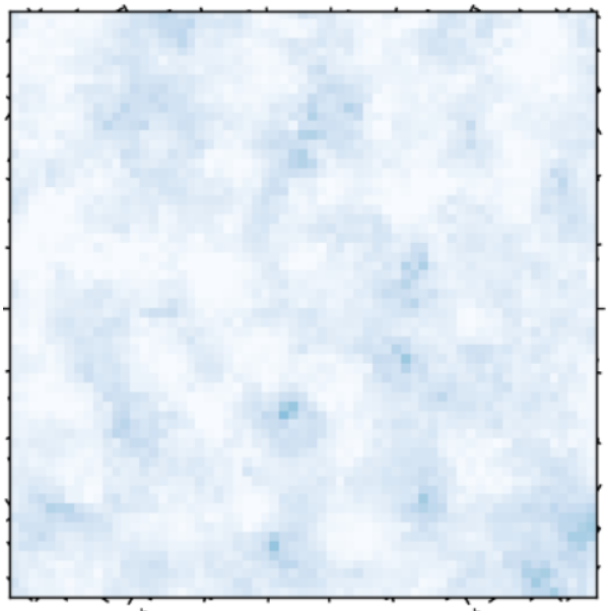

FIG. 15: 6 GHz, redshift bin 9 – 12, contains 37 sources

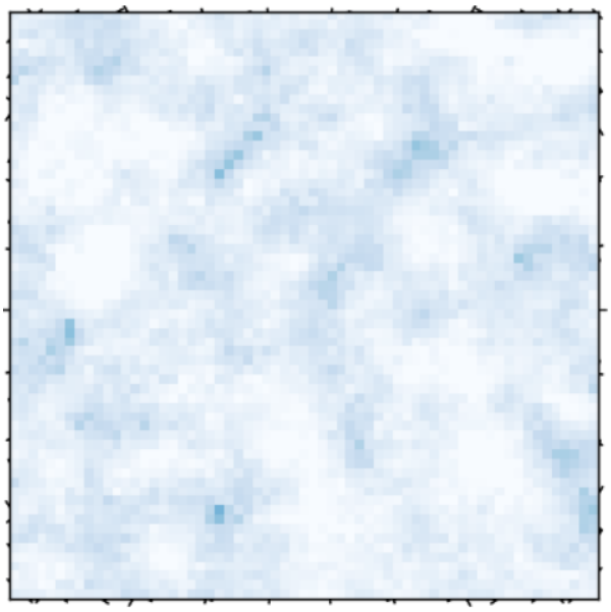

FIG. 16: 3 GHz, redshift bin 9 – 12, contains 43 sources